Marginal Power-Based Maximum Power Point Tracking Control of Photovoltaic System Under Partially Shaded Condition

Mohamad Amin Ghasemi, Hossein Mohammadian Foroushani, and Frede Blaabjerg, *Fellow, IEEE*

***Abstract*—In this article, a two-stage maximum power point tracking algorithm is presented to track the global maximum power point of photovoltaic systems in partially shaded conditions. The proposed tracker uses an intelligent sampling procedure based on a fractional open-circuit voltage method and takes initial samples from the power-voltage characteristic of the photovoltaic array. Then, it determines the marginal array power around each sample. Using these marginal powers, the samples that definitely are not in the vicinity of global maximum power point are eliminated, and neighborhood of these samples are not searched in the global search stage. As a result, the search area gets smaller and global maximum power point is found accurately and rapidly. Furthermore, an algorithm is suggested to estimate module voltage at its maximum power point, which is used in the proposed maximum power point tracker. Eventually, several simulations are carried out through MATLAB/Simulink in order to evaluate the performance of the new tracking method and compare it with recently presented methods. Experimental results are also presented to verify the validity of the developed tracker.**

***Index Terms*—Marginal power, maximum power point (MPP) tracking, partially shaded condition, photovoltaic (PV) array.**

NOMENCLATURE

Parameter	*Description*
A	Diode ideality factor.
K	Boltzmann constant.
q	Electron charge.
T	Temperature in Kelvin.
$I_{\rm PH}$	Photo generated cell current.
I_s	Saturation current.
$I_{\rm sc}$	Short circuit current.
$V_{\rm oc}^{M}$	Module open-circuit voltage.
$V_{\rm MPP}^{M}$	Maximum power point voltage of PV module.
UIC	Uniform Irradiance condition.
$V_{\rm MPP}^{\rm array}$	Maximum power point voltage of array at UIC.
GMPP	Global maximum power point.
V_i	$i \times V_{\rm MPP}^{M}$.
I_i	Array current at V_i.
P_i	Array power at V_i.
P_i^*	Marginal power peak of array around V_i.
N_s	Number of modules in each string of array.
K_s	Maximum number of $V_{\rm MPP}^{M}$ between two samples (Selective).
$N_{\rm sh}$	Number of shaded modules in each string of array.
$N_{\rm in}$	Number of unshaded modules in each string of array.
$V_i^{\rm LP}$	Voltage of array local peak around V_i.
$P_i^{\rm LP}$	Power of array local peak around V_i.
$V_{\rm up}$	The maximum voltage that GMPP can locate.

Manuscript received December 7, 2018; revised March 28, 2019, June 21, 2019, and September 21, 2019; accepted November 1, 2019. Date of publication November 10, 2019; date of current version February 20, 2020. Recommended for publication by Associate Editor K. A. Kim. *(Corresponding author: Mohamad Amin Ghasemi.)*

M. A. Ghasemi is with the Electrical Engineering, Bu Ali Sina University, Hamedan, Iran (e-mail: ma.ghasemi@basu.ac.ir).

H. M. Foroushani is with the Electrical and System Engineering, Washington University in St Louis, St Louis, MI 63130, United States (e-mail: hossein@wustl.edu).

F. Blaabjerg is with Energy Technology, Aalborg University, Aalborg DK-9220, Denmark (e-mail: fbl@et.aau.dk).

Color versions of one or more of the figures in this article are available online at http://ieeexplore.ieee.org.

Digital Object Identifier 10.1109/TPEL.2019.2952972

I. Introduction

PHOTOVOLTAIC (PV) energy systems, especially the grid-connected type, have been commercialized in many countries due to their potential long-term advantages [1]. As a result, researchers now concentrate on the following research areas in this type of PV system: 1) proposing the technologically advanced components; 2) defining control algorithms that are maximizing the energy conversion efficiency of the system, and 3) expanding applications for the PV systems.

In order to guarantee the optimal utilization of large PV arrays under uniform irradiance condition (UIC), traditional maximum power point tracking (MPPT) controllers are used. In general, these methods are classified in close-loop approaches and open-loop approaches. Among close-loop methods, which decrease the steady-state error, hill climbing, perturbation and observation (P&O), and incremental conductance (IC) are the most practical approaches. Among open-loop methods, which improve tracker dynamic response, fractional open-circuit voltage, and fractional short-circuit current are also the most significant types. Popularity of these trackers is actually a result of the simplicity and the low implementation cost [2].

However, one of the significant drawback of the conventional MPPT techniques is the inability to track the maximum power point (MPP) under partially shaded condition (PSC). In PSC, *P–V* characteristic of the PV array usually has multiple peaks, which include one global peak and several local peaks, and traditional MPPT methods fail to track global peak. Given the measurements, which are carried out under real operating

conditions of PV systems, the power loss due to the MPPT failure can be up to 70% [3]. To deal with this severe power loss, researchers developed several modified trackers. MPPT control that uses a periodic scan sequence of the *P–V* curve is frequently employed in commercially available PV power conditioning devices. This method finds the global peak in all cases, but its time-consuming nature decreases tracking efficiency [4]. Some two stages trackers were also presented for tracking of the global peak during PSC. For example, a two-stage method is suggested on the basis of examining the potential MPPs [5]. When the PV power suddenly changes beyond a certain threshold, this tracker calls the global search program. This method finds the new MPP among the local peaks without scanning the entire of the *P–V* curve. However, the proposed tracker uses two unproven concepts to limit the search area. Indeed, when this tracker comes to the local peak that is generating less power than the last observed one, or when the measured oscillation in the array power is more than the certain tolerable power variation during the global search, this tracker gives up searching the remained area in which the MPP might exist. As a result, these two conditions can cause MPPT failure. In [6], array voltage is changed by a linear function after PSC detection. This linear function is based on short-circuit current and open-circuit voltage of the array, and it is claimed that the operating point is moved by this linear change to the vicinity of the global MPP (GMPP). However, this linear change traps the tracker in local peaks in some cases when there are more than two irradiance levels and strings have different shading patterns [4]. In [7], a modified incremental conductance approach is proposed fundamentally on the basis of sequential increasing and decreasing trend of extreme points magnitude, yet this basic assumption is not true in some cases, especially when the partial shading is heavy and number of shaded modules in different strings are not close to each other. In this situation, one small power peak can be surrounded by two large power peaks on each side. Thus, consuming sequential increasing or decreeing trend is not a valid assumption. The proposed method in [8] is a typical two-step MPPT method that has both the ability to find GMPP and better dynamic performance. The proposed method also imposes minimum disturbance to the connected grid. In [9], a MPPT method is presented for PV application. This MPP tracker exploits the inductor characteristic to obtain the PV voltage at GMPP. Then, P&O algorithm is called to track the GMPP. The fuzzy algorithm [10], particle swarm optimization (PSO) [11], [12], firefly algorithm [13], ant-colony optimization [14], artificial bee colony [15], grey wolf optimization [16], and simulated annealing were also used [17]. These intelligent methods are difficult to implement because of the heavy calculation burden and initial point selection, which hinder the application in the commercial PV systems. Also, the chief challenges of these stochastic methods are preventing premature convergence and increasing the convergence speed. In other words, the trade-off between exploitation and exploration is one of the major topics that highly depends on the problem nature [18]. Apart from the proper particle diversification in the new environment, solving dynamic optimization problems also requires modified optimization algorithms, which find the global optimal solution and track the trajectory of the changing global best solution in a dynamic environment [20]. Several methods were presented to alleviate these problems in the PSO approach to some extent [20]–[22].

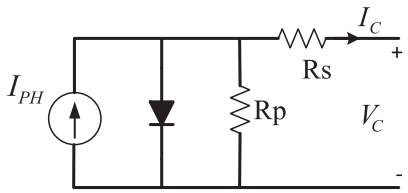

Fig. 1. Equivalent circuit of a PV cell.

Some other deterministic methods have been presented in [23]–[26] which have better performance in comparison to artificial intelligence-based methods. The proposed method in [23] samples the array current in the multiples of $V_{\rm oc}^{M}$. Then, the number of steps, their lengths, and their order in the *I-V* curve of the array are determined by comparing the measured currents against each other. Then, using P&O algorithm, those MPPs are tracked. Finally, the array powers are compared in tracked MPPs, and then GMPP is achieved. In the situation that the number of steps is high, the tracking speed reduces dramatically. Based on the presented method in [24], the *P-V* curve is searched for MPPs by means of the IC algorithm. However, it skips some voltage ranges based on the measured current of the array and highest sampled power. This method has high accuracy, but because of scanning a large part of the *P-V* curve with small steps, tracking speed is low. The presented method in [26] is a modified version of the method in [5], in which the search region is limited knowing short circuit current of array in standard test condition. Therefore, tracking speed and efficiency were improved. The proposed method in [25] has better performance over other deterministic methods. However, this method is complicated, and its implementation is complex.

In this article, a new MPPT method is proposed to track the GMPP under PSC. Cheap implementation, simple implementation, high speed, and high accuracy are the main advantages of the proposed method. The remainder of the article is organized as follows. Section II discusses the characteristics of the PV array in partially shaded conditions. In Section III, the marginal power of each local MPP, which potentially exists near each taken sample, is determined. Also, a novel approach is suggested to estimate the average module voltage at its maximum power point in the developed controller. Afterward, the new MPPT algorithm is introduced, and the used intelligent sampling method is also described in this section. In Section IV, simulation results are presented to evaluate the performance of the proposed algorithm, and the good performance is confirmed by experimental results in Section V. Finally, Section VI concludes this articles.

II. Nonlinear Characteristics of PV Array Under PSC

Solar cell can be modeled with the equivalent circuit that is displayed in Fig. 1. This model includes current source $I_{\rm PH}$, diode D, series equivalent resistance R_s, and parallel equivalent resistance R_P. The relationship of the output voltage (V_c) and

the output current (I_c) can then be represented as

$$I_c = I_{\rm PH} - I_s\left[\exp^{\frac{q(V_c+R_sI_c)}{\rm AKT}} - 1\right] - \frac{V_c + R_sI_c}{R_P} \quad . \qquad (1)$$

The voltage and the current of a PV module can also be related to each other with a relatively similar equation. The module current has its maximum value $(I_{\rm sc}^M)$ at the zero voltage, and it is zero at $V_{\rm oc}^M$. According to the fractional open-circuit voltage method, the maximum module power is achieved at $V_{\rm MPP}^M = K_1 V_{\rm oc}^M$. The coefficient K_1 is usually considered about 0.8, yet its exact value is actually dependent on the module type, temperature, and irradiance level.

PV array includes several series PV modules and several parallel PV modules to provide the desired voltage and current levels. Bypass diodes and blocking diodes are usually connected in parallel to each PV module and series to each string, respectively, to deal with hot-spot problem and current imbalance between strings in array. Commercial PV panels usually include some bypass diodes, and indeed, they do have some modules in one frame. In the rest of the article, PV module title is used for a set of PV cells that are parallel with one bypass diode and is different from PV panel.

When the array has N_s series modules in each of its strings and it is under UIC, the array MPP is approximately located at the $N_s V_{\rm MPP}^M$. However, when the modules receive different irradiance levels during PSC, *P-V* characteristics of the PV array has several peak points because of using bypass diodes in parallel with each module. According to [27] and [28], number of MPPs and their locations during PSC depend on the number of irradiance levels, the difference between the irradiance levels, number of parallel strings, and the shading pattern on the array. To study how a typical array behaves under PSC, let it start with one string under PSC and two different irradiance levels (shaded and unshaded) for the sake of simplicity. $N_{\rm in}$ is the number of unshaded modules in this string which called insulated modules, and $N_{\rm sh}$ is the number of shaded modules $(N_s = N_{\rm in} + N_{\rm sh})$. For currents higher than $I_{\rm sc}$ of shaded modules, the bypass diodes across these $N_{\rm sh}$ shaded modules conduct. In this situation, the maximum power point of string happens when each unshaded module operates at $V_{\rm MPP}^M$. Hence, the first MPP of this string is located at about $N_{\rm in}V_{\rm MPP}^M$. For currents lower than $I_{\rm sc}$ of the shaded modules, unshaded modules operate in approximately constant voltage area close to $V_{\rm oc}^M$. In this situation, the second MPP occurs when the voltage of each shaded module is about $V_{\rm MPP}^M$. As a result, string voltage in its second MPP is greater than $N_s V_{\rm MPP}^M$. In [27] and [28], location estimation of the array MPPs during PSC is explained by considering the PV array as the combination of several parallel groups with different irradiance patterns in general. Group is composed of several strings with identical *I-V* characteristics. The number of extreme points in *P-V* curve of each group curve is equal to the number of irradiance levels on the related group string. Accordingly, if there are two irradiance levels, as in the previous example, then there will be two MPPs in the group *P-V* curve. As explained earlier, these two MPPs occur in different locations. The local MPP voltage, in which the shaded modules are bypassed, $(V^{\rm LP})$ is approximately expressed by

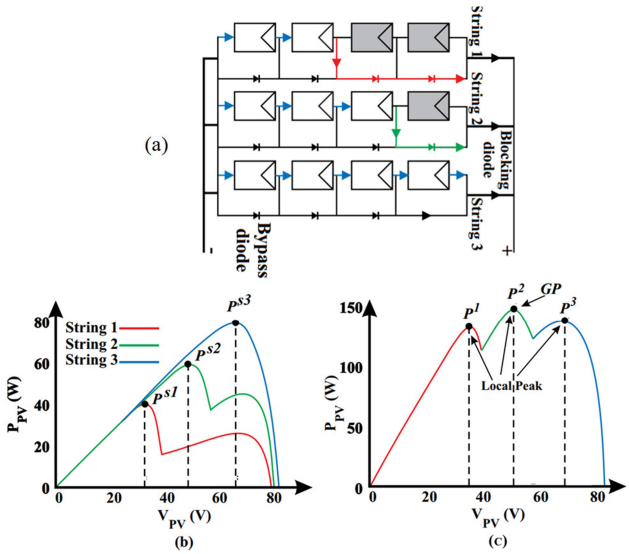

Fig. 2. (a) PV array in PSC: The solar irradiance for the shaded modules and the others are $= 1$ kW/m^2 and $= 0.5$ kW/m^2, respectively. (b) *P-V* curves for each string. (c) *P-V* curve for the entire array.

$$V^{\rm LP} \approx N_{\rm in} V_{\rm MPP}^M. \qquad (2)$$

In practice, (2) can be used to take samples in MPPT. In the rest of article, this sampling method at integer multiples of $V_{\rm MPP}^M$ is called fractional open-circuit voltage (FOCV) sampling method, and the resultant tracker is called FOCV tracker. As an example for the application of FOCV sampling method, Fig. 2(a) demonstrates a PV array that includes three strings $(V_{\rm MPP}^M = 16$ V). Each string is under different shading pattern, so each string is a group and there are three groups totally. The first string, the second string, and the third string consist of two shaded modules, one shaded module, and zero shaded module, respectively. The pertinent *P-V* curves for each of these three strings are depicted in Fig. 2(b). As was predicted, the first string, the second string, and the third string have two MPPs, two MPPs, and one MPP, respectively. Since $N_{\rm in}$ is 2 in string 1 and $V_{\rm MPP}^M = 16$ V, the first peak is observed nearly at the voltage of 32 V. P^{s2} and P^{s3} also occur at nearly 48 and 64 V, respectively. Fig. 2(c) shows the *P-V* curve for the entire groups, which is acquired by scaling the string curves on the current axis. In [28], it is claimed that the position of the string curve peaks P^{s1}, P^{s2}, and P^{s3} are the same as the position of array peaks (P^1 to P^3). Therefore, using FOCV method, samples from the *P-V* curve of the array, according to (2), at $V \approx mV_{\rm MPP}^M$ $(m = 1 : N_s)$ and calls the local search at the sample with the largest power tracks GMPP. However, the position of the peaks P^{s1}–P^{s3} is not the same as the position of the peaks P^1–P^3 in the *P-V* curve of the entire array.

To prove the claim made, the basic concept of the IC method is first reminded. In general, the slope of the *P-V* curve is zero at the MPP, positive on the left of the MPP and negative on the right of the MPP. Taking derivative from array power equation

results in

$$\frac{dP}{dV} = I + V\frac{dI}{dV} \approx I + V\frac{\Delta I}{\Delta V}. \tag{3}$$

Hence, the following equations will be valid around $V = V_{\mathrm{MPP}}^{\mathrm{array}}$

$$\begin{cases} \left|\frac{\Delta I}{\Delta V}\right| = \left|\frac{I}{V}\right|, & V = V_{\mathrm{MPP}}^{\mathrm{array}} \\ \left|\frac{\Delta I}{\Delta V}\right| > \left|\frac{I}{V}\right|, & V > V_{\mathrm{MPP}}^{\mathrm{array}} \\ \left|\frac{\Delta I}{\Delta V}\right| < \left|\frac{I}{V}\right|, & V < V_{\mathrm{MPP}}^{\mathrm{array}} \end{cases}. \tag{4}$$

Now, let it be assumed that there are two strings in the array with different shading patterns, and the first string is under PSC with N_{in} unshaded modules. Thus, the first MPP of this string is approximately located at $N_{\mathrm{in}}V_{\mathrm{MPP}}^{M}$ based on (2). In this voltage, the second string is in the constant current region of its *I-V* curve, so it is in left side of its own MPP. Accordingly, the following equations are resulted by using the IC method in $V = N_{\mathrm{in}}V_{\mathrm{MPP}}^{M}$

$$\begin{cases} \left|\frac{\Delta I_{\mathrm{string1}}}{\Delta V}\right| = \left|\frac{I_{\mathrm{string1}}}{V}\right| \\ \left|\frac{\Delta I_{\mathrm{string2}}}{\Delta V}\right| < \left|\frac{I_{\mathrm{string2}}}{V}\right|. \end{cases} \tag{5}$$

When the two equations in (5) are added together, the resultant inequality is

$$\left|\frac{\Delta I_{\mathrm{string1}}}{\Delta V}\right| + \left|\frac{\Delta I_{\mathrm{string2}}}{\Delta V}\right| < \left|\frac{I_{\mathrm{string1}}}{V}\right| + \left|\frac{I_{\mathrm{string2}}}{V}\right|. \tag{6}$$

When the string currents are added together, the result is the array current (I_{array}), so (6) can be written as

$$\left|\frac{\Delta I_{\mathrm{array}}}{\Delta V}\right| < \left|\frac{I_{\mathrm{array}}}{V}\right|. \tag{7}$$

According to (4) and (7), the voltages of the array MPPs are always more than the voltages of the string MPPs. Thus, when samples are taken from the array *P-V* curve according to the FOCV method, no sample is exactly taken from the array MPPs, and there is always voltage deviation between the sampled voltages and voltages at the actual array MPPs. This sampling deviation is called an intrinsic sampling error in this article. Fig. 2(c) also shows that the intrinsic error between sampled voltages V_1, V_2, and V_3 and the real local MPPs are 1.4, 1.9, and 2.4 V, respectively.

The second problem in using the FOCV method is the dependency of V_{MPP}^{M} on the operating condition. In fact, $V_{\mathrm{MPP}}^{M} = K_1V_{\mathrm{oc}}^{M}$ and the variation in K_1 can be up to 10% while the temperature as well as irradiance is changing [29]. The V_{oc}^{M} also depends on the temperature, and its calculation in a specific time period which is carried out periodically by momentarily shutting down the power converter decreases the power quality significantly. Over the past few years, some methods like pilot cell [30] were proposed to estimate the array open-circuit voltage in a more efficient manner but all to no avail. In the next section, two effective approaches are presented to deal with the problem of not having accurate K_1 and V_{oc} and the intrinsic sampling error.

III. Proposed MPPT Method

The proposed MPPT method is a modified version of FOCV tracker whose two aforementioned deficiencies are resolved in the proposed method. Also, other intelligences are added to increase the speed of MPPT with a decrease in the taken samples. In the following, the details about the modifications are presented, and finally the proposed method is explained.

A. Intrinsic Sampling Error

According to previous arguments, if array voltage samples are taken by (2), then there are always intrinsic error between voltage samples and actual power peak voltages, and the real MPP is generally located at right side of the *i*th sample $(V > V_i = i \times V_{\mathrm{MPP}}^{M})$. Hence, there are differences between the *i*th power sample P_i at V_i and the real local power peak P_i^{LP}. In other words, the peak P_i^{LP} can be presented as

$$P_i^{\mathrm{LP}} = P_i + \Delta P_i. \tag{8}$$

The ΔP_i is a positive uncertain value that depends on different factors. In this article, it is tried to consider its upper limit (ΔP_i^*). Therefore, the modified power sample is defined as

$$P_i^* = P_i + \Delta P_i^*. \tag{9}$$

Modified power sample P_i^* is always greater than or equal to $P_{\mathrm{LM}i}$. P_i^* is the marginal power peak that potentially exists in the right side of V_i. Furthermore, two formulae will be derived to calculate P_i^* for power sample P_i at $V_i (i = 1 : N_s)$, and then, these two formulae will be used in the developed MPP tracker to limit the search area.

1) Estimation of P_i^* for $i = 1 : N_{\mathrm{s}} - 1$: It is known that if there is a step change in array current between V_i and V_{i+1}, then there is a local peak (P_i^{LP}) between V_i and V_{i+1} in *P-V* curve of the array. Otherwise, there is no peak between V_i and V_{i+1}, so there is no need to estimate P_i^* and search this region for GMPP. This step change in the array *I-V* curve is resulted from the step change in the *I-V* curve of one string or the step change in the *I-V* curve of more than one string in general. In both cases, the strings with i unshaded modules per string, which cause the step change in current, can be modeled as the first group and other strings that approximately have constant currents in the vicinity of V_i can be modeled as the second group. Without loss of generality, let it be considered that the *I-V* curve of the array is the sum of two *I-V* curves in the vicinity of this voltage interval $[V_i, V_{i+1}]$. The current of the second curve is a constant current curve as $I = I_{i+1}$ that models the current of the second group strings, and the first curve is its complimentary, as depicted in Fig. 3(a), which models the current of the first group strings.

Accordingly, the array current can be expressed by:

$$I(v) = I_1(v) + I_2(v) = I_1(v) + I_{i+1}, \quad V_i < v < V_{i+1}. \tag{10}$$

Fig. 3(b) shows the *P-V* curve of the array, which is the sum of two corresponding curves, as represented by

$$P(v) = I_1(v)\,v + I_2(v)\,v = P_1(v) + P_2(v). \tag{11}$$

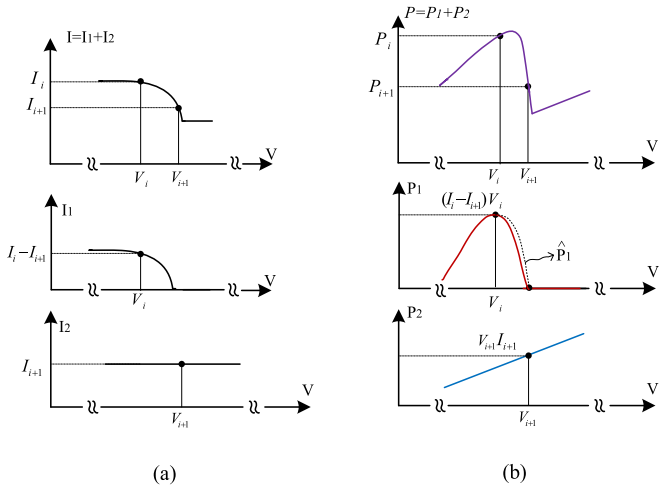

Fig. 3. (a) *I-V* characteristics of both groups in the vicinity of V_i. (b) *P-V* characteristics of both groups of stings in the vicinity of V_i.

The curve of $P_1(v)$ has its maximum at V_i. The curve of $P_2(v)$ is also an increasing function of voltage. With these in mind and according to the presented arguments in Section II, the MPP of the PV array is always located at a voltage larger than V_i. Indeed, the MPP voltage is the solution to the following equation:

$$\left|\frac{dP_1(v)}{dv}\right| = \left|\frac{dP_2(v)}{dv}\right| \tag{12}$$

where $dP_2(v)/dv$ is equal to I_{i+1}, and $P_1(v)$ is approximately in the form of a second-order polynomial between its peak at V_i and V_{i+1} as follows:

$$P_1(v) = a(v - V_i)^2 + b. \tag{13}$$

The values of P_1 at V_i and V_{i+1} are

$$\begin{cases} P_1(V_i) = V_i(I_i - I_{i+1}) \\ P_1(V_{i+1}) = 0. \end{cases} \tag{14}$$

Solving (13) with the two constraints given by (14) results in calculating unknown parameters a and b as

$$\begin{cases} a = -\frac{V_i(I_i - I_{i+1})}{(V_{i+1} - V_i)^2} \\ b = V_i(I_i - I_{i+1}). \end{cases} \tag{15}$$

Thus, (11) can be written as

$$P(v) \approx \hat{P}(v) = a(v - V_i)^2 + b + vI_{i+1}. \tag{16}$$

After taking derivative from (16), the optimal array voltage can be calculated by

$$V_{\mathrm{MPP}}^{\mathrm{array}} = \frac{I_{i+1} + 2aV_i}{-2a}. \tag{17}$$

Now, if the calculated $V_{\mathrm{MPP}}^{\mathrm{array}}$ by (17) is replaced in (16), the marginal maximum power of array P_i^* on right side of sample voltage V_i is calculated as

$$P_i^* = a\left(\frac{I_{i+1} + 2aV_i}{-2a} - V_i\right)^2 + b + \left(\frac{I_{i+1} + 2aV_i}{-2a}\right) I_{i+1}. \tag{18}$$

2) Estimation of $\boldsymbol{P_i^*}$ for $\boldsymbol{i = N_s}$: Finding the exact location of the rightmost MPP is possible, in practice, by the method presented in [1]. However, this method is valid for a single string array, and it is very hard to determine the location of the rightmost peak exactly for an array in general. Here, the method proposed in [31] is used with some modification to estimate $\boldsymbol{P_{Ns}^*}$. It is clear that each string in a PV array either does not have a shaded module or has at least one shaded module. In the former case, the related strings have their power peaks close to V_{Ns}. In the latter case, each string has two power peaks each of which has location varying with the change in the number of shaded modules in that string [1]. Location of the first power peak was discussed earlier. As was mentioned before, the location of the second peak is at a voltage greater than V_{Ns}. PV arrays comprise these two types strings mentioned, so the rightmost peak of a PV array always locates after V_{Ns}. On the other hand, based on reasoning of [1] and [8], it can be easily shown that the step in string current is finished before $N_{\mathrm{in}}V_{\mathrm{oc}}^M$ and second power peak locates before $N_{\mathrm{in}}V_{\mathrm{oc}}^M + (\mathrm{Ns} - N_{\mathrm{in}})V_{\mathrm{MPP}}^M$. Since a PV array includes strings, these reasoning are true for a PV array too. Suppose that all the step changes in array current, except to the last one, are at the left side of voltage sample V_n, and V_{ls} is the voltage sample where the one to last step change in current occurs in $[V_{\mathrm{ls}} \;\; V_{\mathrm{ls}+1}]$. Accordingly, the rightmost peak of the array locates before $V_n + (\mathrm{Ns} - \mathrm{ls})V_{\mathrm{MPP}}^M$. In other words, the upper voltage limit for the rightmost peak can be determined by

$$V_{\mathrm{up}} = V_n + (N_s - l_s)V_{\mathrm{MPP}}^M = V_n + V_{\mathrm{Ns}} - V_{\mathrm{ls}}. \tag{19}$$

Moreover, the array current has a decreasing trend with the voltage increase, so the array current at the last power peak is not greater than I_{Ns}. Thus, the last power peak is never greater than $V_{\mathrm{up}}I_{\mathrm{Ns}}$, and the marginal power for the last power sample can be calculated by

$$P_{\mathrm{Ns}}^* = V_{\mathrm{up}}I_{\mathrm{Ns}}. \tag{20}$$

This equation can be used simply for $i > \mathrm{Ns}$ as

$$P_i^* = V_{\mathrm{up}}I_i, \quad i > \mathrm{Ns}. \tag{21}$$

B. Module Maximum Power Voltage V_{MPP}^M Estimation

Based on earlier discussions, an important challenge of using the FOCV method is that both values of V_{oc}^M and K_1, and consequently V_{MPP}^M, depend on the operating condition. An important contribution of the proposed method here is the idea of estimating the $V_{\mathrm{MPP}}^M = K_1V_{\mathrm{oc}}^M$ in the MPPT control loop. In this method, V_{MPP}^M is estimated while neither V_{oc}^M nor K_1 are equal to their actual values. Actual value of V_{MPP}^M is estimated using MPP location. According to (2), any minor change in V_{MPP}^M, obviously, makes a small change in the MPP location which is continuously tracked during the fixed shading pattern. Therefore, the information of the GMPP location and the corresponding N_{in}, which was discovered by the global search program, is used to obtain actual value of V_{MPP}^M by

$$V_{\mathrm{MPP}}^M \approx \frac{V_{\mathrm{MPP}}^{\mathrm{array}}}{N_{\mathrm{in}}} \tag{22}$$

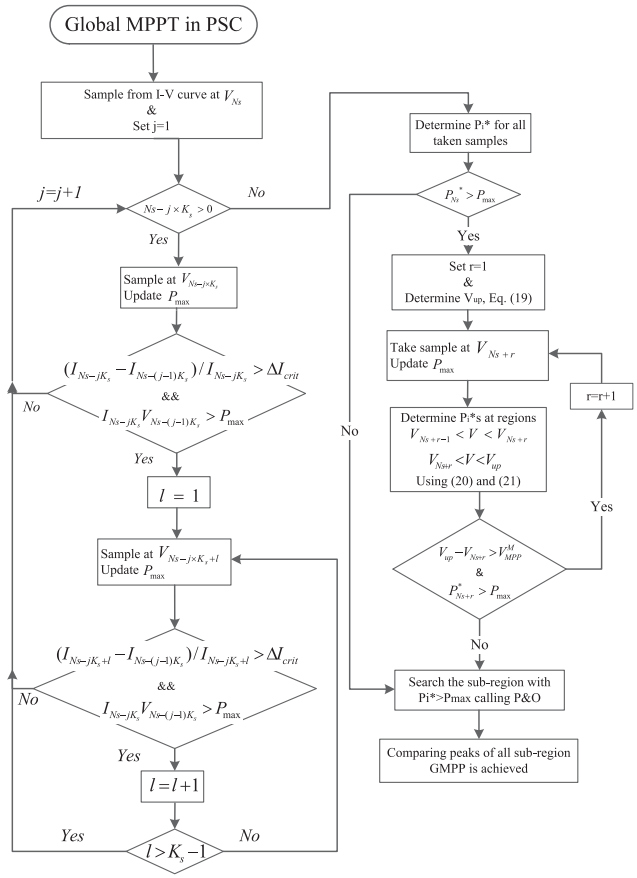

Fig. 4. Flowchart of the proposed algorithm.

where $V_{\rm MPP}^{\rm array}$ and $N_{\rm in}$ are the information in the last shading pattern (UIC that its corresponding $N_{\rm in}$ is N_s can be used at start step). As an example, if the shading pattern is what Fig. 2(c) depicts, then $V_{\rm MPP}^{\rm array}$ and $N_{\rm in}$ would be 50.8 and 3, and $V_{\rm MPP}^{M}$ would be estimated as 16.93 V (which is a little more than its actual value) and $V_{\rm MPP}^{M}$ is used in the next PSC occurrence in FOCV sampling method. Moreover, further critical observations and simple argument revealed that using $V_{\rm MPP}^{M}$ of (22) in FOCV method is beneficial because the initial samples are taken closer to the local extreme power points of the PV array.

C. Proposed MPPT Algorithm

It was mentioned that the proposed MPPT method is a modified version of FOCV method whose explained deficiencies have been resolved. Also, some other intelligences are added to the sampling mechanism that are described in the following. The flowchart of the proposed MPP tracker is shown in Fig. 4. The variation in shading pattern usually leads to sudden large power change. Hence, when the P&O is tracking the MPP during local search, if the power change around the operating point is greater than a certain threshold $\Delta P_{\rm crit}$ between two consecutive samples, the change in the shading pattern is detected. However, there are situations where no big change in the array power is observed. Therefore, some papers propose triggering the GMPPT method periodically to handle these situations [24].

According to the proposed tracker, when the change in the shading pattern is detected, the global search subroutine is called, and the first one sample is taken from $V_{N_s}=N_sV_{\rm MPP}^{M}$. Another sample is taken at $V_{(N_s-K_s)}=(N_s-K_s)\times V_{\rm MPP}^{M}$, where K_s is a selective integer number; it is at least two times smaller than N_s to divide the voltage search region to more than two subregions. Then, the following steps are done on voltage subregion $[V_{(N_s-K_s)}\quad V_{\rm Ns}]$. At first, two conditions are checked: 1) if there is a step change in current more than a critical value $(\Delta I_{\rm crit})$ between $[V_{(N_s-K_s)}\quad V_{\rm Ns}]$ (it is worthy to note that, according to [23], appropriate value for $\Delta I_{\rm crit}$ is 10%) and 2) if $V_{\rm Ns}I_{N_s-K_s}$ is bigger than $P_{\rm max}$ ($P_{\rm max}$ is maximum power of samples taken after change in PSC, and it is updated with any new taken sample). It is clear that there is no MPP in the subregions with no step change in current, and this subregion is eliminated in the rest of the search. Also, if $V_{\rm Ns}I_{N_s-K_s}$ is smaller than $P_{\rm max}$, considering that array power is confidently lower than $V_{\rm Ns}I_{N_s-K_s}$ between $[V_{(N_s-K_s)}\quad V_{\rm Ns}]$, global MPP of the array is not in this subregion, and this subregion is eliminated in the rest of the global search too. Therefore, if both conditions are valid, another sample is taken at $V_{N_s-K_s+1}=V_{(N_s-K_s)}+V_{\rm MPP}^{M}$. Then, two aforementioned conditions are checked in $[V_{N_s-K_s+1}\quad V_{N_s}]$, and if needed (both conditions are valid), another sample is taken at $V_{N_s-K_s+2}$. This sampling procedure continues until either at least one of two conditions is rejected or the last sample is taken at V_{N_s-1}. After that, another sample is taken at $V_{(N_s-2K_s)}$, and the above-mentioned steps are done on subregion $[V_{N_s-2K_s}\quad V_{N_s-K_s}]$. This procedure is done for subregions $[V_{N_s-3K_s}\quad V_{N_s-2K_s}]$, $[V_{N_s-4K_s}\quad V_{N_s-3K_s}]$, and etc., until the last subregion is considered $[V_1\quad V_{N_s-([N_s/K_s]-1)K_s}]$ (interior [] is the symbol of integral part operator).

Based on above-discussed sampling method, suppose that totally Ms samples have been taken at multiple integer of $V_{\rm MPP}^{M}$ until now and their maximum power is $P_{\rm max}$. Accordingly, the voltage region $V_{\rm MPP}^{M}<V<N_sV_{\rm MPP}^{M}$ is divided into $\rm Ms-1$ small subregions.

In the small subregions with step change in current, marginal power peaks (P_i^*) are estimated using (18). Also, there is another subregion $(V_{\rm Ns}<V<V_{\rm up})$ whose marginal power peak $(P_{\rm Ns}^*)$ is also estimated using (20). Then, $P_{\rm Ns}^*$ is compared with $P_{\rm max}$. If $P_{\rm Ns}^*$ is less than $P_{\rm max}$, the tracker does not take excessive samples. On the other hand, if $P_{\rm Ns}^*$ is greater than $P_{\rm max}$, tracker takes more samples at multiples of $V_{\rm MPP}^{M}$, starting from $V_{\rm Ns+1}$, until it surpasses $V_{\rm up}$ in (19). Then, it calculates P_i^* for all new samples by (21).

At the final step, all P_i^*s are compared with $P_{\rm max}$. If P_i^* is greater than $P_{\rm max}$, P&O algorithm is called with large step size to search the vicinity of V_i rapidly, and the corresponding local peak is tracked. Then, all tracked local peaks are compared to achieve the location of GMPP. After that, the operating point is placed in the GMPP, and P&O is called with a small step size to reduce steady-state error of the MPPT controller.

To illustrate the method more, let us consider Fig. 5. In this case, a PV array with 12 series modules in each string is considered, and the tracker takes seven samples from the PV array. Then, it finds the maximum power sample, which is the sample at V_9 and $P_{\rm max}=P_9$. Then, based on the presented

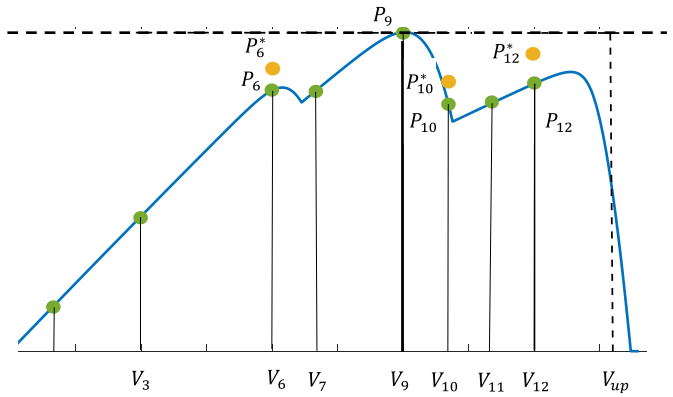

Fig. 5. Using marginal power to limit the search area. P_i^*s are marginal power peaks estimated and P_is are power samples.

descriptions about the proposed method, the marginal powers are estimated for the samples at V_6 and V_{10} by (18) and for V_{12} by (20). Then, $P_{\max}$ and modified samples (P_6^*, P_{10}^*, and P_{12}^*) are compared. None of the modified samples are greater than $P_{\max}$, thus P&O method is called to search the vicinity of the finalized sample (V_9), and then the global power peak is finally tracked.

D. Closed-Loop Control of the Boost Converter

In the simplest method, the input voltage of boost converter V_{in} can be changed by an open-loop control of the duty cycle. However, the dynamic response of the boost converter to step change in the duty cycle has large dynamics. This large dynamic response is due to resonance manner between $\boldsymbol{C_{in}}$ and $\boldsymbol{L}$ of the boost converter and its low damping factor, and equivalent negative dynamic resistance of the PV array. Also, the output voltage of boost converter and the input current of boost converter, which is PV array output current, are considered disturbance to the system that their changes can affect the response of boost converter in control of its input voltage (V_{pv}). To resolve the deficiency mentioned about open-loop control of the boost converter, a closed-loop control structure shown in Fig. 6 is used. The PV voltage V_{pv} is fed back and compared with the reference voltage V_{ref} which is determined by the MPPT controller. Then, using a proportional-integral (PI) controller, the proper dynamic response is achieved. It should be mentioned that using two cascade control loops, including inductor current control loop as inner loop and boost input voltage control loop as outer loop, can decrease settling time of converter considerably.

IV. Simulation Results

The suggested MPPT algorithm is verified by several simulations in MATLAB/Simulink environment. The simulated array has three strings with four panels in each string and is simulated in various PSCs. The PV panels of the array are SunPower SPR-205 BLK that has parameters listed in Table I. This PV panel has three bypass diodes, so it can be considered as three modules each of which has only one bypass diode across. Thus, each panel is

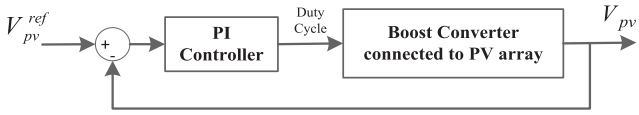

Fig. 6. Closed-loop voltage control of boost converter.

TABLE I
Simulated PV Module Frame Parameters in Standard Condition

Parameter	Symbol	Value
Maximum Power	P_{MPP}	205W
Maximum Power Current	I_{MPP}	5.13A
Maximum Power Voltage	V_{MPP}	40V
Short Circuit Current	I_{sc}	5.53A
Open Circuit Voltage	V_{oc}	47.8V
Voltage Drop of Bypass Diode	V_d	0.8V

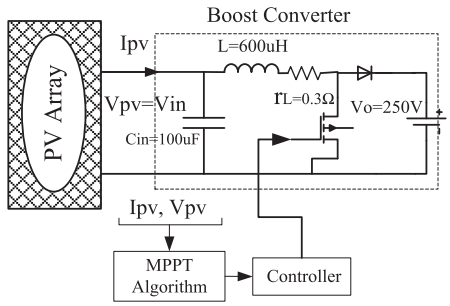

Fig. 7. Simulated boost converter connected to PV Array.

considered as three modules with nominal value of $V_{\text{MPP}}^M = 13.3$ V, and each string of the simulated array includes 12 modules. The simulation setup also comprises a boost converter connected to the PV array, a shown in Fig. 7. The switching frequency of the boost converter is 20 kHz, and proportional and integral coefficients of the PI controller are $K_p = 0$ and $K_I = -2.4$, respectively.

According to [32], the maximum settling time of the system step response is calculated for the simulated system. Since this time is about 7 ms in the simulated system, the tracker sampling time is considered 10 ms in all simulations. Also, the parameter K_s is considered 3 in the simulations. It is worthy to note that using a larger value for K_s can increases the tracking speed. ΔP_{crit} is considered 5% of the array power at the operating point. Also, ΔI_{crit} was selected 5% of array current at taken voltage sample, conservatively lower than the proposed value in [23]. The *P-V* curves of the simulated PV array in five irradiance condition are shown in Fig. 8. At first, the array is in UIC then its irradiance condition and shading pattern changes from PSC1 to PSC4 consecutively with time period of 0.5 s.

Under UIC, all PV panels receive the same irradiance level equal to 0.9 kW/m^2. Then, the array is partially shaded such that one PV panel (three modules) from string 1 and one PV panel from string 2 are shaded and irradiance level of shaded modules are 0.3 kW/m^2 (named PSC1). Shade expands and

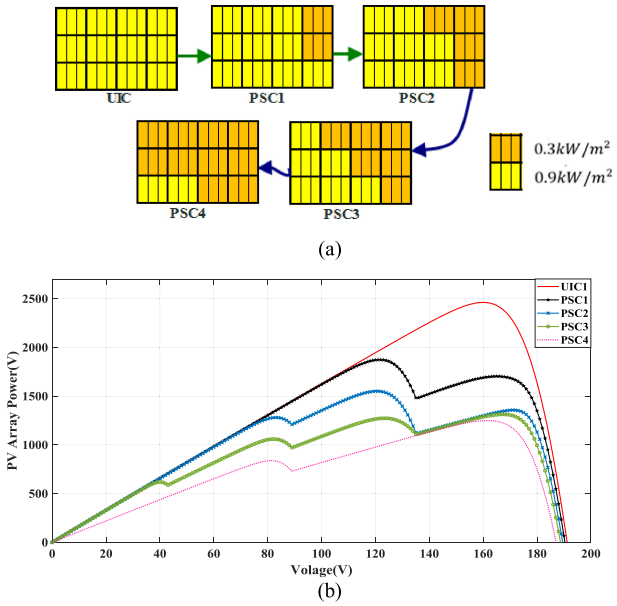

Fig. 8. (a) Shading patterns on the simulated PV array and (b) its *P-V* curves in five irradiance conditions.

another PV panel from string 1 and one PV panel from string 3 are also shaded (named PSC2). Likewise, one PV panel from strings 1 and 2 are also added to shaded panels (PSC3). Finally, under PSC4, all PV panels of string 1 and 2 and one PV panel from string 3 are shaded. Shading patterns on the simulated PV array and the corresponding *P-V* curves are shown in Fig. 8, whose corresponding GMPPs are (160 V, 2462 W), (122 V, 1874 W), (121 V, 1551 W), (165 V, 1287 W), and (162 V, 1250 W), respectively.

To illustrate how the proposed method works, let it be supposed that the array is under UIC. In UIC, MPP of array is at 160 V, and $V_{\rm MPP}^{M}$ is estimated 13.3 V by using (22). After occurrence of PSC1 and detection of power change more than 5%, the proposed method takes two samples at 160 and 120 V. As two aforementioned conditions are valid within [120, 160 V], so another sample is taken at 133.3 V. Again, two conditions are valid in $[133.3, 160\ \text{V}]$, so another sample is also taken at 146.6 V. Then, according to the proposed method, the next sample is taken at $V_{\text{Ns}-2k_s} = 80$ V, and since there is no current step change in $[80,\ 120\,\text{V}]$, no extra sample is taken in this subregion. With the same procedure, the next sample is taken in $V_{\text{Ns}-3k_s} = 40\,\text{V}$. There is no current step change in $[40,\ 80\,\text{V}]$; therefore, the next sample is taken at 13.3 V. Since no current step change is observed in $[13.3,\ 40\,\text{V}]$, the sampling is terminated.

Among the seven samples taken, the $P_{\max}$ is 1871 W, which is at $V_9 = 120\,\text{V}$. Accordingly, only the subregions [120, 146.6 V] and $[160\,\text{V}\ V_{\rm up}]$ should be searched for GMPP. Based on (20), $V_{\rm up}$ and $P_{\rm Ns}^{*}$ are determined as $V_{\rm up} = 146.6 + 160 - 133.3 = 173.3\,\text{V}$ and $P_{\rm Ns}^{*} = 173.3{*}10.56 = 1830\,\text{W}$, respectively, which is lower than $P_{\max}$. Hence, sampling is terminated and P_i^{*} is determined for $V_{10} = 133.3\,\text{V}$ equal to $P_{10}^{*} = 1430\,\text{W}$, which is also lower than $P_{\max}$. Therefore, GMPP will be in $[120,\ 133.3\,\text{V}]$. Therefore, the global search step is terminated and P&O algorithm is called which tracks the exact GMPP at $V = 123$ V. Operation of the proposed method including voltage and power of the array is depicted in Figs. 9(d) and 10(d).

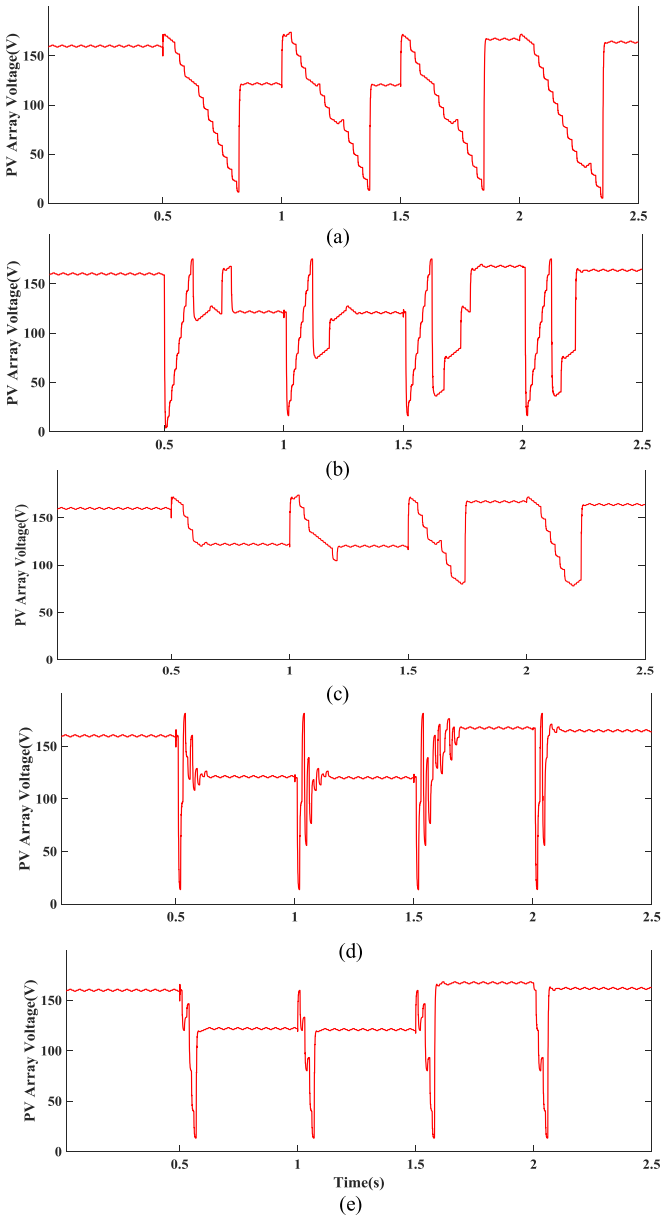

Fig. 9. Simulation results, including array voltage changes during operation of five GMPP methods, (a) presented method in [5], (b) presented method in [23], (c) presented method in [26], (d) presented method in [25], and (e) the proposed method in this article.

In order to compare the performance of the proposed method with some prior art methods in this field, the presented deterministic methods in [25], [5], [26], and [23] are selected, which are among the best methods in this field. In what follows, the simulations mainly compare the trackers' functionality under the five consecutive irradiance conditions. Description about the selected methods was presented in Section I and extra details can be found in corresponding papers.

The presented simulation results show that all methods have tracked GMPP in all four PSCs. The tracking times for four

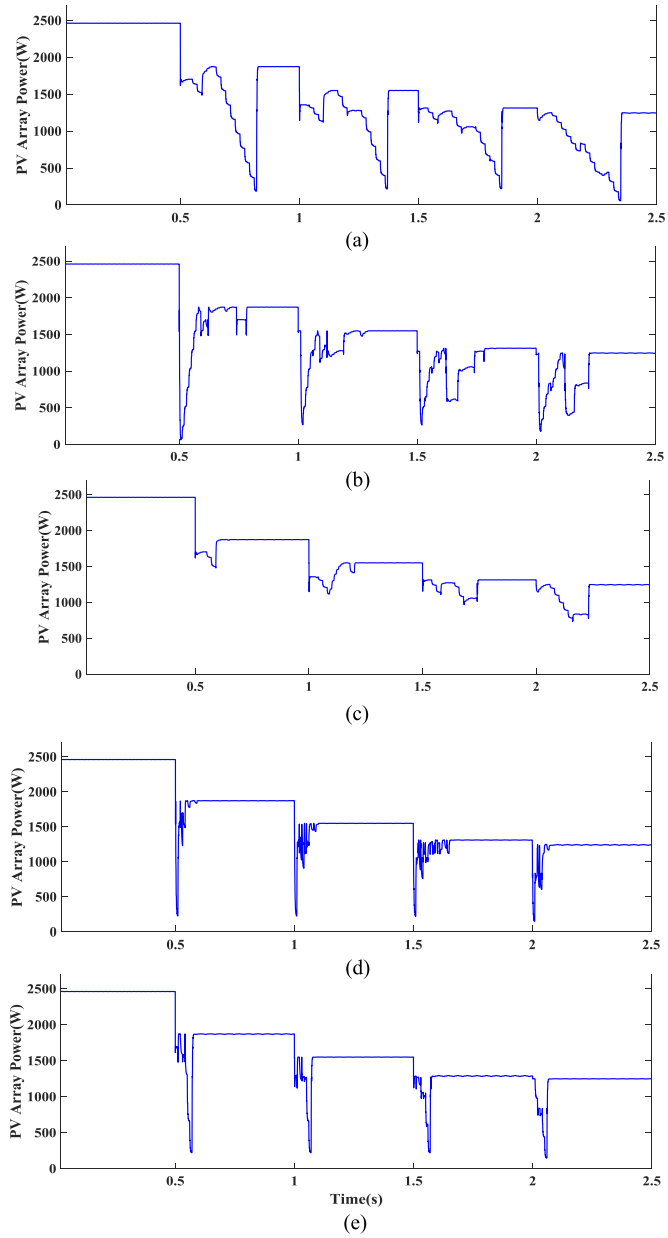

Fig. 10. Simulation results including array power changes during operation of five GMPP methods, (a) presented method in [5], (b) presented method in [23], (c) presented method in [26], (d) presented method in [25], and (e) the proposed method in this article.

methods in four PSCs are presented in Table II. Total energy loss, which is the difference between the maximum energy that could be extracted and the energy extracted by the GMPPT algorithms, during the algorithms' operations (0–2.5s), is also presented in Table II. It can be seen that the proposed method has obvious superiority over the methods in [23], [26], and [5] in the field of speed and energy loss. It also has relative superiority over the presented method in [25].

It should be mentioned that the presented results in Figs. 9 and 10 are sample results, and further PSCs have been simulated for comparison of the proposed method with the selected methods. Table III summarizes the relative comparison of five

TABLE II
TRACKING TIME AND TOTAL ENERGY LOSS FOR FIVE SIMULATED METHODS IN FOUR PSCS

		Proposed Method	Method in [23]	Method in [5]	Method in [26]	Method in [25]
Tracking time (ms)	PSC1	70	180	320	110	90
	PSC2	70	260	370	210	100
	PSC3	70	230	350	230	150
	PSC4	60	220	350	220	70
Total Energy Loss between 0 to 2.5s (j)		140	400	620	180	170

TABLE III
COMPARISON OF FIVE MPPT METHODS

Criterion	Proposed Method	Method in [23]	Method in [5]	Method in [26]	Method in [25]
Convergence speed	Very high	Medium	Low	Low	High
Accuracy	High	High	High	High	High
Total energy loss	Very low	Medium	High	Low	Low
Needed parameters	N_s	N_s and V_{oc}^{M}	N_s and V_{oc}^{M}	N_s, V_{oc}^{M} and I_{sc}	V_{oc}^{array}
Implementation complexity	Medium	Low	Low	Medium	High

methods using well-known criteria including accuracy, convergence speed, total energy loss, implementation complexity, and needed parameters. The proposed method in this article takes initial samples in special points and uses a specific region-based logic to limit the search area, so it requires fewer samples. Accordingly, the speed of tracking is improved and as a result energy loss decreases in comparison to other simulated methods. Also, the proposed method only requires number of modules in string, so it is superior to other methods that need open-circuit voltage as well.

Finally, it is noted that, similar to other GMPP trackers, the proposed GMPP tracker determines the GMPP based on the taken samples from the *P-V* curve of array in the corresponding PSC. Therefore, if during the operation of GMPP tracker (during sampling of global search), which lasts few tens of millisecond, irradiance or PS condition change, then the taken samples, during global search step, will from two or more PSCs, and the determined point as GMPP might be wrong.

V. EXPERIMENTAL RESULTS

To verify the performance of the proposed method further, the experimental setup, as shown in Fig. 11, is developed. The setup comprises a boost converter that is paralleled with six series 12 V batteries with a total voltage of more than 72 V. These series batteries keep the output voltage of the boost converter constant.

The boost converter has the specifications presented in the Table IV, and its duty cycle is controlled by using one Arduino Board- AVR ATMEGA328P-16 MHz microcontroller in a closed-loop control structure. Current and voltage sensors

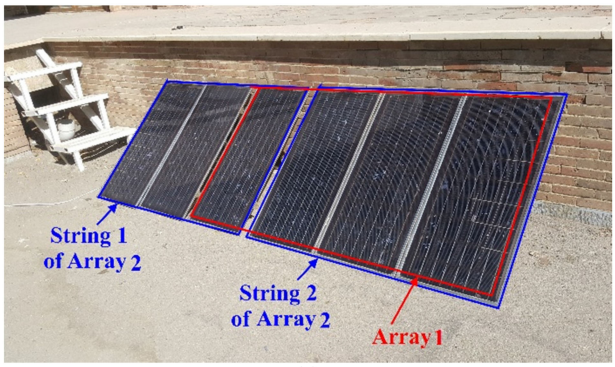

(a)

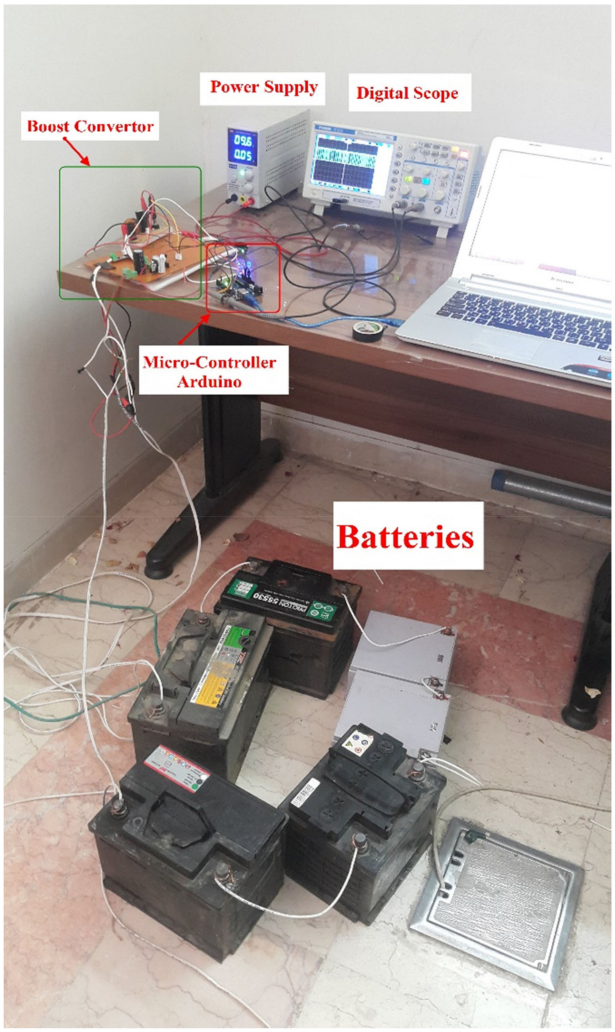

(b)

Fig. 11. Overview of the experimental setup: (a) PV array and (b) power stage.

TABLE IV
EXPERIMENTAL BOOST CONVERTER PARAMETERS

Parameter	Symbol	Value
Input Capacitor	C_i	100 uF
Inductor	L	0.4 mH
Switching Frequency	f_s	25 kHz
Output Voltage	V_o	74 V

TABLE V
EXPERIMENTAL PV MODULE PARAMETERS IN STANDARD CONDITION

Parameter	Symbol	Value
Maximum Power	P_{MPP}	37W
Maximum Power Current	I_{MPP}	2.35A
Maximum Power Voltage	V_{MPP}	15.8V
Short Circuit Current	I_{sc}	2.55A
Open Circuit Voltage	V_{oc}	19.5V

used in experimental setup are ACS712 (Hall effect-based linear current sensor with suitable accuracy is used and its total output error is lower than 1.5%) and HCPL7840, respectively. The tracker sampling time is considered 10 ms, which is greater than the maximum converter settling time in the experiment with a discretized integrator controller with $K_I = -3$ (discretization sampling time of the controller is 200 us). Input of the boost converter is connected to a PV array. Experiments were performed with two different PV arrays configurations [see Fig. 11(a)].

1) Array 1 has one string which has four panels (eight series modules).
2) Array 2 has two parallel strings each of which has three panels (six series modules).

Panel characteristics are included in Table V. As each panel has two bypass diodes, then each string in array 1 and array 2 has eight series modules and six series modules, respectively. A semi dark nylon sheet was used to cover some modules and create shading during the experiment. Based on short-circuit current of the panels, lower irradiance level and higher irradiance level in tests are about 0.74 and 0.2 kW/m^2, respectively.

It should be mentioned that running the P&O tracking algorithm for Array1 under UIC tracked the MPP at $V = 56$ V. However, according to Table V, which shows the PV module parameters in standard condition ($S = 1\,\mathrm{kW/m^2}$, $T = 25^{\circ}\mathrm{C}$), MPP should be at $V = 4 \times 15.8 = 63.2$ V. Therefore, V_{MPP}^{M} was updated to 7 V based on (22) (V_{MPP}^{M} was 14 for the panel equivalently).

First experiment was performed with the first PV array configuration and one panel was deliberately made shaded. *I-V* and *P-V* characteristics of PV array during PSC were obtained with a small step change in the converter duty cycle and are shown in Fig. 12(a).

It should be mentioned that the aim of the experimental test is confirmation of the proposed global search algorithm, therefore, the test procedure is considered as follows. At first, while the array was shaded, the voltage of PV array was set to 56 V, which was voltage of MPP under UIC (reference voltage of the boost converter voltage control loop set to 56 V). Then, the proposed global search stage of MPPT algorithm was activated by pushing a bottom on the control board. It is noted that K_s was considered 3. Accordingly, during the global search step, six samples were taken at $V = 56$, 35, 42, 49, 14, and 7 V based on the proposed algorithm. Based on the taken samples, the GMPP was found to be around $V_6 = 42$ V, then P&O algorithm was activated and tracked the exact GMPP at 42 V. Tracking array voltage, current,

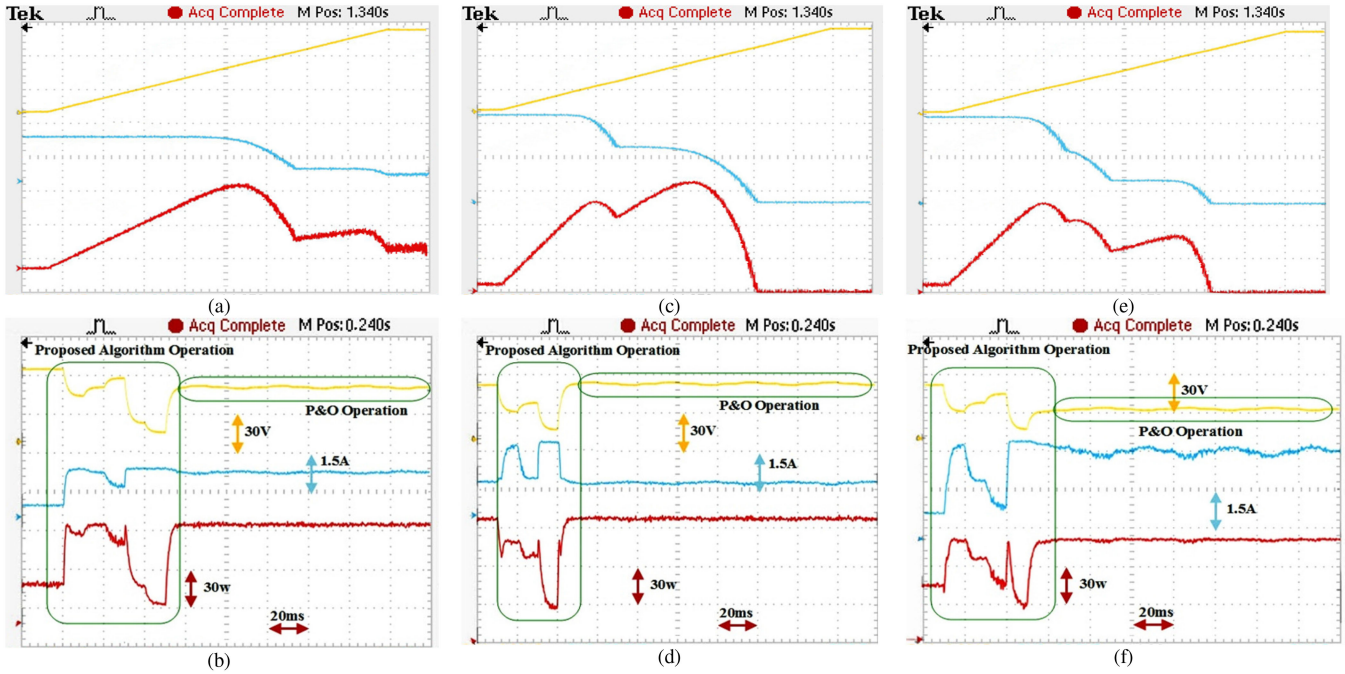

Fig. 12. Experimental results: (a) characteristics of the first array under PSC. (b) Tracking array voltage, current, and power with the proposed approach for the first array under PSC. (c) Characteristics of second array under its first PSC (d) Tracking array voltage, current, and power with the proposed approach for the second array under its first PSC. (e) Characteristics of the second array under its second PSC. (f) Tracking array voltage, current, and power with the proposed approach for second array under its second PSC.

and power with the proposed approach for the first array under PSC are shown at Fig. 12(b). As was expected, GMPP happens at multiple of module optimum voltage when array has one string ($42 = 6 \times 7$).

Second experiment was performed with the second PV array configuration under two different PSC conditions as follows.

Case 1: In first PSC scenario, one panel was shaded in first string. Thus, first string had two shaded modules and four unshaded modules. Second string also had two unshaded modules. *I-V* and *P-V* characteristics of partially shaded PV array during PSC are shown in Fig. 12(c). Similar to the previous test, while the array was shaded, the voltage of the PV array was set to 42 V, which was voltage of the array at MPP under UIC. Then, the proposed global search stage of MPPT algorithm (K_s was considered 3) was activated by pushing a bottom on the control board. During the global search, four samples were taken by MPP tracker at $V = 42$, 21, 28, and 7 V based on the proposed algorithm. Based on the taken samples the location of GMPP was found to be in right side of $V_{\rm NS} = V_6 = 42$ V, then P&O algorithm was activated and tracked GMPP at $V = 44$ V. Tracking array voltage, current, and power with the proposed approach for second array under this PSC are shown at Fig. 12(d).

Case 2: In second PSC scenario, one and half panel (three modules) was shaded in first string and one panel (2 modules) was shaded in the second string. Thus, first string had three shaded modules and three unshaded modules. Second string also had two shaded modules and four unshaded modules. *I-V* and *P-V* characteristics of partially shaded PV array during this PSC are shown in Fig. 12(g). At first, the voltage of PV array was set to 42 V, which was voltage of the array at MPP under UIC. Then, the proposed global search stage of MPPT algorithm (K_s was considered 3) was activated by pushing a bottom on the control board.

During the global search, five samples were taken by the proposed tracker at $V = 42$, 21, 28, 35, and 7 V based on the proposed algorithm. Based on the taken samples, the location of GMPP was found to be in right side of 21 V. Then P&O algorithm was activated and tracked exact location of GMPP at 23 V. Tracking array voltage, current, and power with the proposed approach for second array under this PSC are shown at Fig. 12(h). As was expected, GMPP happens at right side of multiple of module optimum voltage when array has more than one string (23 is larger than $21 = 3 \times 7$)

VI. Conclusion

A new MPPT method was presented for tracking the MPP in partially shaded condition. Without complicating converter design by making severe undesirable transients, this software-based method applies fractional open-circuit voltage concept and takes the minimum samples to detect potential MPPs. Then, it uses an analytic condition for the reliable elimination of the excess search area without taking further samples, so the proposed tracker finds the MPP rapidly but reliably in all cases. Moreover, the calculation of the module maximum power voltage is usually a matter of challenge to the trackers needing this voltage. An efficient approach was proposed to estimate the adequate approximation of this voltage in the MPPT controller, so the module maximum power voltage estimation diminishes

sampling error. The simulation and experimental results also confirm the better performance of the tracker in comparison to some prior art methods. Apart from the reliable detection of the MPP in PSCs, the convergence speed of the presented method is high, the steady-state error is acceptable and the structure of the new MPPT algorithm is simple.

REFERENCES

[1] J. Ahmed and Z. Salam, "An improved method to predict the position of maximum power point during partial shading for PV arrays," *IEEE Trans. Ind. Informat.*, vol. 11, no. 6, pp. 1378–1387, Dec. 2015.

[2] G. Petrone, G. Spagnuolo, R. Teodorescu, M. Veerachary, and M. Vitelli, "Reliability issues in photovoltaic power processing systems," *IEEE Trans. Ind. Electron.*, vol. 55, no. 7, pp. 2569–2580, Jul. 2008.

[3] F. Liu, Y. Kang, Y. Zhang, and S. Duan, "Comparison of P&O and hill climbing MPPT methods for grid-connected PV converter," in *Proc. 3rd IEEE Conf. Ind. Electron. Appl.*, 2008, pp. 804–807.

[4] E. Koutroulis and F. Blaabjerg, "A new technique for tracking the global maximum power point of PV arrays operating under partial-shading conditions," *IEEE J. Photovolt.*, vol. 2, no. 2, pp. 184–190, Apr. 2012.

[5] H. Patel and V. Agarwal, "Maximum power point tracking scheme for PV systems operating under partially shaded conditions," *IEEE Trans. Ind. Electron.*, vol. 55, no. 4, pp. 1689–1698, Apr. 2008.

[6] Y. Ji, D. Jung, J. Kim, J. Kim, T. Lee, and C. Won, "A real maximum power point tracking method for mismatching compensation in PV array under partially shaded conditions," *IEEE Trans. Power Electron.*, vol. 26, no. 4, pp. 1001–1009, Apr. 2011.

[7] K. S. Tey and S. Mekhilef, "Modified incremental conductance algorithm for photovoltaic system under partial shading conditions and load variation," *IEEE Trans. Ind. Electron.*, vol. 61, no. 10, pp. 5384–5392, Oct. 2014.

[8] M. A. Ghasemi, H. M. Foroushani, and M. Parniani, "Partial shading detection and smooth maximum power point tracking of PV arrays under PSC," *IEEE Trans. Power Electron.*, vol. 31, no. 9, pp. 6281–6292, Apr. 2016.

[9] S. Selvakumar, M. Madhusmita, C. Koodalsamy, S. P. Simon, and Y. R. Sood, "High-speed maximum power point tracking module for PV systems," *IEEE Trans. Ind. Electron.*, vol. 66, no. 2, pp. 1119–1129, Feb. 2019.

[10] B. N. Alajmi, K. H. Ahmed, S. J. Finney, and B. W. Williams, "A maximum power point tracking technique for partially shaded photovoltaic systems in microgrids," *IEEE Trans. Ind. Electron.*, vol. 60, no. 4, pp. 1596–1606, Apr. 2013.

[11] M. Miyatake, M. Veerachary, F. Toriumi, N. Fujii, and H. Ko, "Maximum power point tracking of multiple photovoltaic arrays: A PSO approach," *IEEE Trans. Aerosp. Electron. Syst.*, vol. 47, no. 1, pp. 367–380, Jan. 2011.

[12] H. Li, D. Yang, W. Su, J. Lü, and X. Yu, "An overall distribution particle swarm optimization MPPT algorithm for photovoltaic system under partial shading," *IEEE Trans. Ind. Electron.*, vol. 66, no. 1, pp. 265–275, Jan. 2019.

[13] K. Sundareswaran, S. Peddapati, and S. Palani, "MPPT of PV systems under partial shaded conditions through a colony of flashing fireflies," *IEEE Trans. Energy Convers.*, vol. 29, no. 2, pp. 463–472, Jun. 2014.

[14] K. Sundareswaran, V. Vigneshkumar, P. Sankar, S. P. Simon, P. S. R. Nayak, and S. Palani, "Development of an improved P&O algorithm assisted through a colony of foraging ants for MPPT in PV system," *IEEE Trans. Ind. Informat.*, vol. 12, no. 1, pp. 187–200, Feb. 2016.

[15] J. S. Goud, R. Kalpana, and B. Singh, "A hybrid global maximum power point tracking technique with fast convergence speed for partial-shaded PV systems," *IEEE Trans. Ind. Appl.*, vol. 54, no. 5, pp. 5367–5376, Sep./Oct. 2018.

[16] S. Mohanty, B. Subudhi, and P. K. Ray, "A new MPPT design using grey wolf optimization technique for photovoltaic system under partial shading conditions," *IEEE Trans. Sustain. Energy*, vol. 7, no. 1, pp. 181–188, Jan. 2016.

[17] S. Lyden and M. E. Haque, "A simulated annealing global maximum power point tracking approach for PV modules under partial shading conditions," *IEEE Trans. Power Electron.*, vol. 31, no. 6, pp. 4171–4181, Jun. 2016.

[18] Z.-H. Zhan, J. Zhang, Y. Li, and H. S.-H. Chung, "Adaptive particle swarm optimization," *IEEE Trans. Syst., Man, Cybern., Part B (Cybern.)*, vol. 39, no. 6, pp. 1362–1381, 2009.

[19] S. Yang and C. Li, "A clustering particle swarm optimizer for locating and tracking multiple optima in dynamic environments," *IEEE Trans. Evol. Comput.*, vol. 14, no. 6, pp. 959–974, Dec. 2010.

[20] Y.-H. Liu, S.-C. Huang, J.-W. Huang, and W.-C. Liang, "A particle swarm optimization-based maximum power point tracking algorithm for PV systems operating under partially shaded conditions," *IEEE Trans. Energy Convers.*, vol. 27, no. 4, pp. 1027–1035, Dec. 2012.

[21] K. Ishaque, Z. Salam, M. Amjad, and S. Mekhilef, "An improved particle swarm optimization (PSO)–based MPPT for PV with reduced steady-state oscillation," *IEEE Trans. Power Electron.*, vol. 27, no. 28, pp. 3627–3638, Aug. 2012.

[22] K. Ishaque and Z. Salam, "A deterministic particle swarm optimization maximum power point tracker for photovoltaic system under partial shading condition," *IEEE Trans. Ind. Electron.*, vol. 60, no. 8, pp. 3195–3206, Aug. 2013.

[23] A. Ramyar, H. Iman-Eini, and S. Farhangi, "Global maximum power point tracking method for photovoltaic arrays under partial shading conditions," *IEEE Trans. Ind. Electron.*, vol. 64, no. 4, pp. 2855–2864, 2017.

[24] Y. Wang, Y. Li, and X. Ruan, "High accuracy and fast speed MPPT methods for PV string under partially shaded conditions," *IEEE Trans. Ind. Electron.*, vol. 63, no. 1, pp. 235–245, Jan. 2016.

[25] M. A. Ghasemi, A. Ramyar, and H. Iman-Eini, "MPPT method for PV systems under partially shaded conditions by approximating I–V curve," *IEEE Trans. Ind. Electron.*, vol. 65, no. 5, pp. 3966–3975, May 2018.

[26] C. Manickam, G. R. Raman, S. I. Ganesan, and N. Chilakapati, "Efficient global maximum power point tracking technique for a partially shaded photovoltaic string," *IET Power Electron.*, vol. 9, no. 14, pp. 2637–2644, 2016.

[27] H. Patel and V. Agarwal, "MATLAB-based modeling to study the effects of partial shading on PV array characteristics," *IEEE Trans. Energy Convers.*, vol. 23, no. 1, pp. 302–310, Mar. 2008.

[28] A. Kouchaki, H. Iman-Eini, and B. Asaei, "A new maximum power point tracking strategy for PV arrays under uniform and non-uniform insolation conditions," *Solar Energy*, vol. 91, pp. 221–232, 2013.

[29] N. Mutoh, M. Ohno, and T. Inoue, "A method for MPPT control while searching for parameters corresponding to weather conditions for PV generation systems," *IEEE Trans. Ind. Electron.*, vol. 53, no. 4, pp. 1055–1065, Jun. 2006.

[30] G. Hart, H. Branz, and C. Cox III, "Experimental tests of open-loop maximum-power-point tracking techniques for photovoltaic arrays," *Solar Cells*, vol. 13, pp. 185–195, 1984.

[31] M. A. Ghasemi, M. Parniani, S. F. Zarei, and H. M. Foroushani, "Fast maximum power point tracking for PV arrays under partial shaded conditions," in *Proc. 18th Eur. Conf. Power Electron. Appl.*, 2016, pp. 1–12.

[32] N. Femia, G. Petrone, G. Spagnuolo, and M. Vitelli, "Optimization of perturb and observe maximum power point tracking method," *IEEE Trans. Power Electron.*, vol. 20, no. 4, pp. 963–973, Jul. 2005.

Mohamad Amin Ghasemi received the B.Sc. degree from Tehran University, Tehran, Iran, in 2008, and the M.Sc. and Ph.D. degrees from the Sharif University of Technology (SUT), Tehran, Iran, in 2010 and 2016, respectively, all in electrical engineering.

He is currently an Associate Professor with the School of Electrical Engineering, Bu-Ali Sina University, Hamadan, Iran. His current research interests include modeling and control of power system, micro grid, and renewable energy sources.

Hossein Mohammadian Foroushani received the B.Sc. degree from the Isfahan University of Technology (IUT), Esfahan, Iran, in 2010, M.Sc. degree from Sharif University of Technology (SUT), Tehran, Iran, in 2012, both in electrical engineering, second M.Sc. degree in engineering data analytics and statistics from Washington University, St Louis, MI, USA, in 2019. He is currently working toward the Ph.D. degree in electrical engineering, Washington University, St. Louis, MI, USA.

He is a Graduate Research Assistant with Neuroinformatics Research Group, Mallinckrodt Institute of Radiology, St. Louis School of Medicine, Washington University. His research interests include control systems, statistical signal processing, machine learning, deep learning, imaging for information inference and decision making, measurement data modeling, algorithms for hypothesis testing, detection and estimation, classification, prediction, performance analysis, and bounds.

Frede Blaabjerg (S'86–M'88–SM'97–F'03) received the Ph.D. degree in electrical engineering, Aalborg University, Aalborg, Denmark, in 1995.

He was with ABB-Scandia, Randers, Denmark, from 1987 to 1988. He became an Assistant Professor in 1992, an Associate Professor in 1996, and a Full Professor of Power Electronics and Drives in 1998. In 2017, he became a Villum Investigator. He is Honoris Causa with University Politehnica Timisoara (UPT), Romania and Tallinn Technical University (TTU) in Estonia. His current research interests include power electronics and its applications such as in wind turbines, PV systems, reliability, harmonics, and adjustable speed drives. He authored or coauthored more than 600 journal papers in the fields of power electronics and its applications, and four monographs and editor of ten books in power electronics and its applications.

Dr. Blaabjerg was the recipient of 31 IEEE Prize Paper Awards, the IEEE PELS Distinguished Service Award in 2009, the EPE-PEMC Council Award in 2010, the IEEE William E. Newell Power Electronics Award 2014, the Villum Kann Rasmussen Research Award 2014, and the Global Energy Prize in 2019. He was the Editor-in-Chief of the IEEE TRANSACTIONS ON POWER ELECTRONICS from 2006 to 2012. He has been the Distinguished Lecturer for the IEEE Power Electronics Society from 2005 to 2007 and for the IEEE Industry Applications Society from 2010 to 2011 as well as 2017–2018. Since 2019, he serves as a President of the IEEE Power Electronics Society. Also, he is the Vice-President of the Danish Academy of Technical Sciences. He is nominated in 2014–2018 by Thomson Reuters to be between the most 250 cited researchers in engineering in the world.